Enhancement of Bovine Bone Ablation Assisted by a Transparent Liquid Layer on a Target Surface

Hyun Wook Kang, Ho Lee, Shaochen Chen, and Ashley J. Welch

Abstract—The purpose of this study was to investigate the laser-induced ablation of bovine bone assisted by a transparent liquid layer on top of the target surface. A Q-switched Nd:YAG laser was used to ablate bovine *tibia* at various energy levels. Distilled water was applied to the sample surface in order to examine the role of a transparent liquid layer during the ablation. Plasma generation and transient acoustic waves were monitored to identify dominant mechanisms involved in the ablation process. Ablation efficiency was measured from the cross-sectional tomography acquired by optical coherence tomography (OCT). Ablation with a liquid layer lowered the damage threshold and enhanced both the laser-induced acoustic excitation and the ablation efficiency, which saturated at higher radiant exposures. The enhanced ablation of the liquid-assisted process is primarily due to photomechanical effects associated with explosive vaporization and plasma confinement. The saturation of the pressure amplitude and ablation efficiency was attributed to increased plasma shielding.

Index Terms—Ablation, acoustic wave, explosive vaporization, laser-induced plasma, plasma confinement, Q-switched Nd:YAG, shockwave.

I. INTRODUCTION

LASERS HAVE been of interest as a feasible alternative in orthopedic surgery since extensive studies for the potential use of lasers for osteotomy procedures began in the 1970s [1], [2]. Standard tools in orthopedics such as saws, milling-machines, and mechanical drills induce severe mechanical vibrations and hemorrhage whereas lasers generally have significant advantages, allowing noncontact intervention, controlled bone excision, free-cut geometry, hemostatic and aseptic effects, and minimal invasiveness [3]. Due to a strong absorption of infrared radiation by high water content and Amide I/II bands in bone tissue, several lasers such as Excimer, Ho:YAG, HF, Er:YAG, CO_2, and FEL have been investigated for surgical application in bone cutting, and their characteristics of bone ablation with various wavelengths and modes have been reported [4]–[9]. Since most lasers tested for osteotomy produced long pulse durations (i.e., > tens of microseconds), a temperature rise in the laser-affected zone is induced with minimal acoustic waves; therefore, material removal is thought to be initiated by photothermal mechanisms [10], [11].

Recent studies demonstrated augmented ablation efficiency by application of a transparent liquid layer on the target surface (termed the "wet condition") [12], [13]. If the damage threshold is defined as the initial surface deformation, then, in the regime slightly above the damage threshold, the efficiency is promoted mainly by increased optical-acoustic coupling and the photomechanical effect in association with explosive vaporization in the strongly superheated liquid layer [14]. Additionally, the liquid-assisted process lowered the damage threshold by 20%–40% along with the augmentation of ablation performance, compared with the direct ablation (termed the "dry condition") [14]. At a high radiant exposure regime, it was reported that the laser-induced plasma is confined in the liquid layer, consequently inducing higher acoustic and shock waves than the dry condition [15], [16]. The enhanced mechanical wave emission imposes significant effects on the mechanical response of the target surface, resulting in more material removal.

Previous studies were conducted mostly with metal samples, and the near-threshold regime and plasma regime were investigated independently [12]–[16]. To the best of our knowledge, this study provides the first experimental report to test laser ablation in liquid confinement on biological bone tissues. In this study, we tested the hypothesis that ablation of biological tissues, especially bovine bone, could be enhanced by increased photomechanical effects, which possibly result from plasma confinement along with the explosive vaporization of a liquid layer. A Q-switched Nd:YAG laser with a short pulse was used with various energy settings. Ablation efficiency was compared for bone samples in air and water environments as a function of radiant exposure with single and multiple pulses. By measuring plasma formation and acoustic wave propagation, the role of a liquid layer during the ablation process was examined.

II. MATERIALS AND METHODS

A. Specimen

Bovine *tibia* obtained from a local slaughter house was used for the laser-tissue ablation experiment. The connective tissue and periosteum were peeled away from the bone specimen, and the sample was rinsed in tap water for approximately 10 min to remove hemocytes. To obtain uniform size samples (1.5×2.5 cm), bone osteotomy was performed using a standard handsaw. The surface was polished using sandpaper with a grain size of 30 μm, maintaining the flat surface of the samples with a constant thickness of approximately 4 mm. Once all of the samples were prepared, they were stored in a saline solution at 4 °C 24 h prior to experimentation, possibly minimizing the change of hydration state of the tissue. In order to perform liquid-assisted ablation, a plastic (Depron) ring with 1-mm

H. W. Kang and A. J. Welch are with the Department of Biomedical Engineering, University of Texas, Austin, TX 78712 USA (e-mail: wookiedokie@mail.utexas.edu; welch@mail.utexas.edu).

H. Lee is with the School of Mechanical Engineering, Kyungpook National University, Daegu 702-701, South Korea (e-mail: holee@knu.ac.kr).

S. Chen is with the Department of Mechanical Engineering, University of Texas, Austin, TX 78712 USA (e-mail: scchen@mail.utexas.edu).

TABLE I
OPTICAL, THERMAL, MECHANICAL PROPERTIES FOR WATER AND BONE [17]–[23]

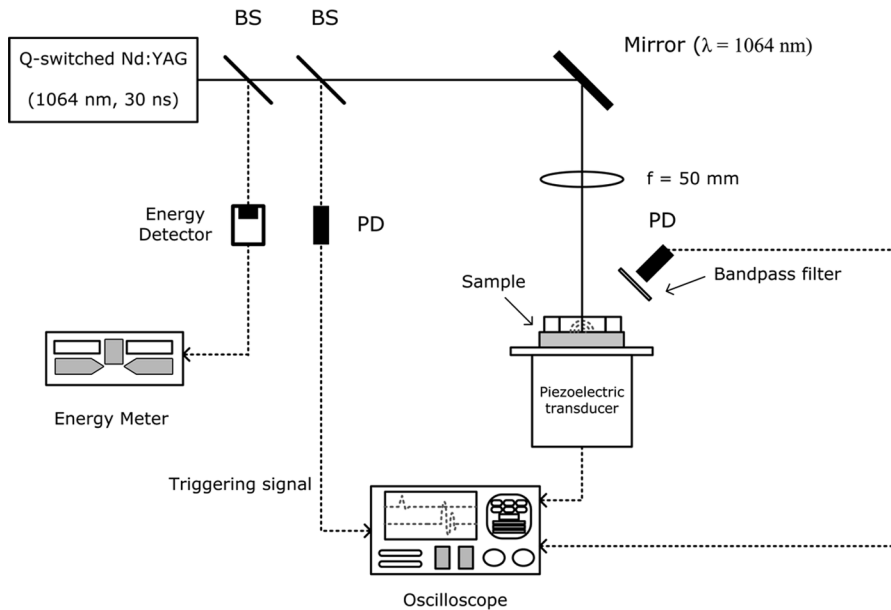| Material Properties	Water	Bone
Optical Absorption Coefficient (cm^{-1})	0.13	N/A
Thermal Conductivity (W/m·K)	0.611	0.373 – 0.496
Fracture Toughness (MPa/m$^{1/2}$)	N/A	2.0 – 5.6
Speed of Sound (m/s)	1481	2000 – 3441

Fig. 1. Schematic of an experimental setup to measure plasma formation and acoustic transients using a Q-switched Nd:YAG laser system. BS: beam splitter; PD: photodetector.

thickness was attached on top of a sample surface to maintain a consistent liquid layer thickness. Prior to laser-pulse irradiation, distilled water was deposited inside the ring. The absorption coefficient of water at the wavelength of interest (1064 nm) was 0.13 cm^{-1}, so that the water layer was relatively transparent with insignificant light absorption [17], [18]. Optical, thermal, and mechanical properties of the target materials are provided in Table I.

B. Laser Source and Delivery

A number of craters were created on bone samples using a Q-switched Nd:YAG laser (Contiuum Surelite II10, Santa Clara, CA). The 1064-nm laser emitted full-width at half-maximum (FWHM) pulses of approximately 30 ns. The applied pulse energy ranged from 11 to 393 mJ, and either one, ten, or 20 pulses were applied with a repetition rate of 1 Hz. A schematic illustration for ablation experiments with the Q-switched Nd:YAG is presented in Fig. 1. Two beam splitters were placed in the beam path; one was used to monitor the pulse energy and the other to achieve a triggering signal. The laser pulse was reflected at an angle of 90° using a 1064-nm BK 7 mirror (CVI laser, Albuquerque, NM). By using a convex CaF$_2$ lens with a

focal length of 50 mm, the laser beam was focused on the surface of the target sample with a spot diameter of 150 μm, which was determined from a knife-edge measurement. The spot size was defined as the distance between 10% and 90% clip points without multiplying the width adjust factor (0.552 $\sqrt{2}$) which is used for the estimation of the $1/e^2$ diameter of a Gaussian beam [24]. An energy detector (PE25BB-DIF, Ophir Optronics Inc., Danvers, MA) was used to monitor the applied pulse energy during the experiment. A fast Si photodetector (1-ns rise time, DET210, Thorlabs, NJ) was used to produce a triggering signal for a digital oscilloscope (Hewlett Packard *Infinium*, Colorado Springs, CO), which measured the temporal profile of plasma and acoustic transients.

C. Plasma and Acoustic Wave Detection

To monitor plasma formation during the ablation process, a fast photodetector with a bandpass filter rejecting 1064 nm was placed approximately 3 cm above the irradiated spot. The breakdown process was detected by eye and confirmed by a photodetector. The laser-induced acoustic wave was monitored experimentally using a commercial piezoelectric transducer (model WAT-04, Science Brothers, Inc., Houston, TX). The
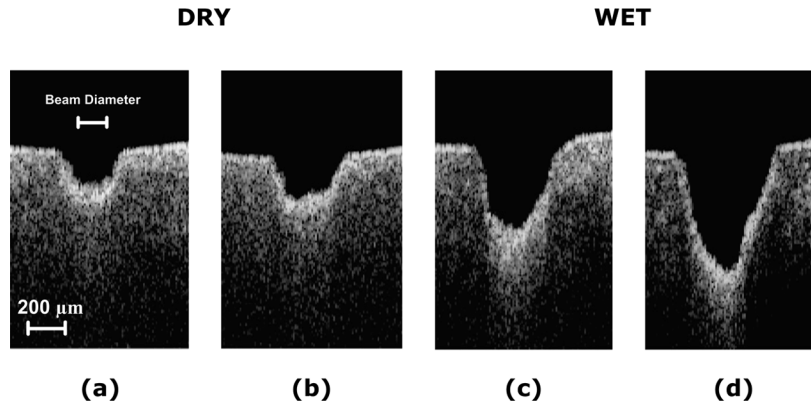
DRY **WET**

Fig. 2. Vertical cross-sectional images of laser-induced craters with a Q-switched laser with 20 pulses for a dry case at the radiant exposure of (a) 14.9 J/mm^2 and (b) 22.2 J/mm^2 and a wet case at (c) 14.9 J/mm^2 and (d) 22.2 J/mm^2.

transducer was mounted below the target, and a 1-mm-thick plastic ring was attached on the transducer surface. During the experiment, the ring was filled with distilled water in order to maintain impedance match between the sample and the transducer. The transducer contained a lithium niobate element calibrated by the manufacturer over a bandwidth up to 100 MHz.

D. Ablation Efficiency

Ablation craters were produced with ten and twenty pulses of various radiant exposures for the purpose of comparing ablation efficiency between dry and wet cases. In order to maintain a consistent liquid layer thickness, distilled water was deposited after each laser pulse. Laser-induced craters were examined using an Optical Coherence Tomography (OCT) system ($\lambda_o = 1290$ nm, $\Delta\lambda = 42$ nm, and $P = 2.2$ mW) with lateral and axial resolution of ~ 20 μm to obtain quantitative ablation dimensions [25], [26]. A series of vertical cross-sectional images (i.e., direction parallel to laser beam propagation) were obtained over the entire crater. The step-size between images was 35 μm. Crater depth and ablation volume were estimated from the OCT cross sections. Craters produced with a single pulse were also observed with an optical microscope to evaluate the damage threshold for each case.

III. RESULTS

Fig. 2 displays the OCT cross-sectional images of the bone samples at 14.9 and 22.2 J/mm^2. Samples were ablated with 20 pulses for both conditions. The craters induced by wet ablation showed larger crater depth and higher ablation volume than those of dry ablation. The laser pulse produced relatively rough and irregular contours. Dimensions of ablation craters for dry and wet cases are compared in Fig. 3. Ten and twenty pulses with various radiant exposures were applied to the samples. Regardless of the radiant exposure, both ablation depth and volume increased with the number of pulses. Crater depth and volume of wet ablation were up to three and six times greater than those of dry condition, respectively. The result shows that the ablation depth and volume increased rapidly as the radiant exposure increased to 8.9 J/mm^2, but, with higher radiant exposure, the rate of increase in ablation performance began to diminish.
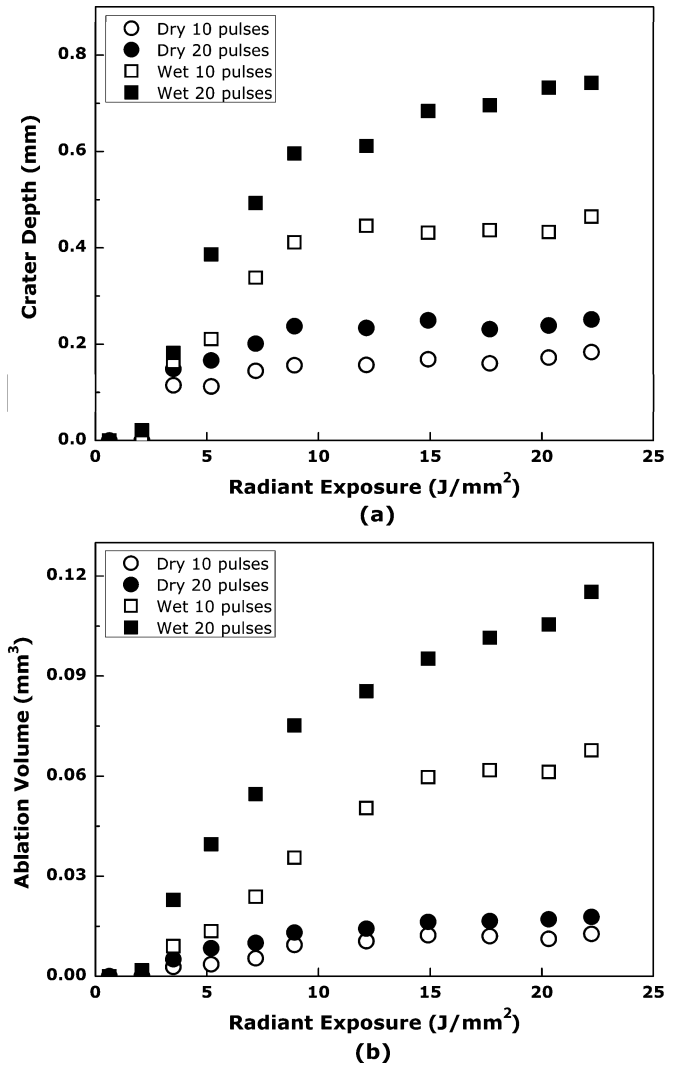

Fig. 3. Comparison of ablation efficiency for dry and wet ablation as a function of radiant exposure with 10 and 20 pulses: (a) crater depth and (b) ablation volume.

The observation with an optical microscope for single-pulse damage (ablation) thresholds for both cases is shown in Fig. 4. From the microscope images, we could estimate the damage-
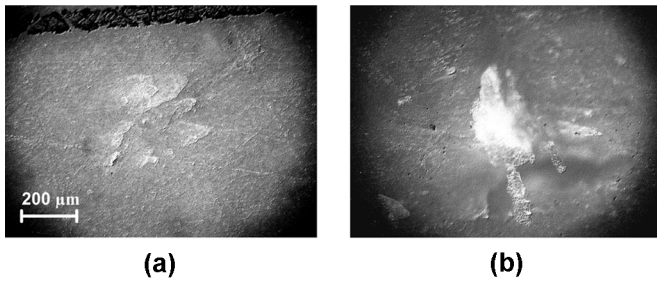
Fig. 4. Top-view images of bovine bone for (a) dry damage threshold ($H = 3.5$ J/mm^2) and (b) wet damage threshold ($H = 2.1$ J/mm^2).

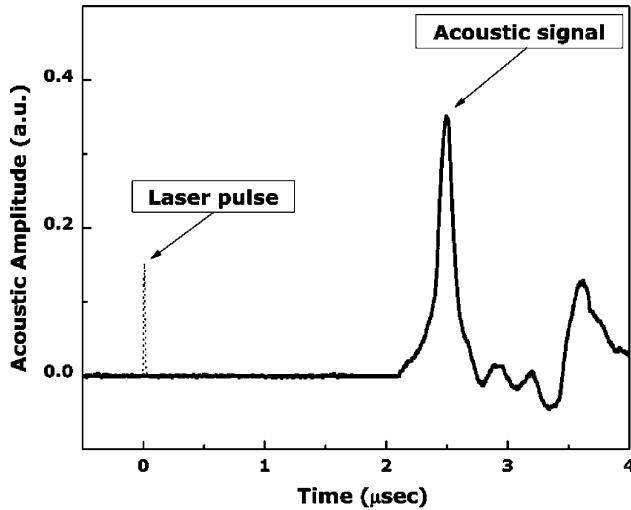

Fig. 5. Acoustic signal measured by a piezoelectric transducer during single-pulse ablation in water produced with 22.2 J/mm^2.

Fig. 6. Temporal behaviors of transient pressure for (a) dry and (b) wet ablation. Note the difference in scale for dry and wet ablation.

threshold radiant exposure at which the morphological deformation started on the surface. The damage thresholds for dry and wet ablation occurred at 3.5 and 2.1 J/mm^2, respectively. Irradiated samples for both cases had randomly propagating cracks at the surface, indicating the mechanical effect during ablation. In particular, the wet image exhibited material removal along with the mechanically induced crack, compared with the dry, which showed little/no removal.

A typical trace of the acoustic transducer is shown in Fig. 5 (single-pulse, wet ablation at $H = 22.2$ J/mm^2, where H is the radiant exposure). The laser pulse was triggered at 0 μs. The acoustic transient was generated approximately 2.1 μs after the onset of the laser pulse. The speed of sound for bovine bone was found to range from 2000 to 3441 m/s, which is dependent on bone density [3]. The time for shock-wave propagation through the bone sample and 1-mm water layer for impedance match can be roughly evaluated by the following equation:

$$t_{\text{shock}} = \frac{d_{\text{bone}}}{c_{\text{bone}}} + \frac{d_{\text{water}}}{c_{\text{water}}} \qquad (1)$$

where t_{shock} is the total propagation time (s), d_{bone} and d_{water} are the sample and layer thickness (m) respectively, and c_{bone} and c_{water} are the speed of sound (m/s) for each material. By using Table I, the propagation time was calculated to range from
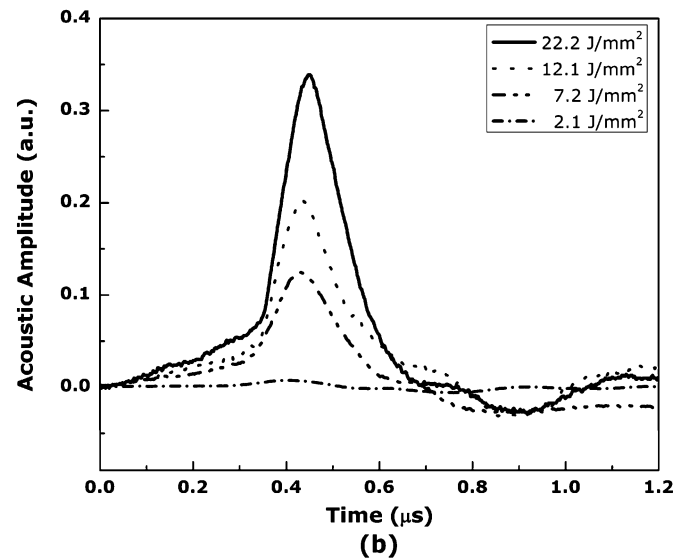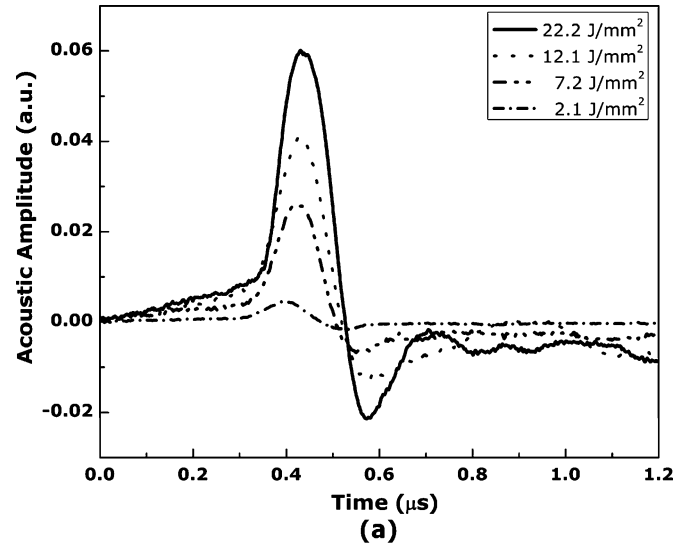
1.84 to 2.68 μs, which corresponded to the measured onset of the acoustic wave at 2.1 μs.

The signatures of the pressure pulse for dry and wet ablation were investigated at various radiant exposures ranging from 0.6 to 22.2 J/mm^2 and are compared in Fig. 6. In the dry condition, the acoustic wave was composed of compressive pressure followed by a tensile wave. The acoustic shape of the wet condition mainly consisted of a compressive part within 1 μs along with a peak amplitude up to six times greater and a compressive wave two to three times longer in duration. The peak acoustic amplitudes of the two conditions are compared in Fig. 7 as a function of radiant exposure. The threshold radiant exposures for the acoustic excitation were identical for both dry and wet conditions at 2.1 J/mm^2. However, the wet ablation produced a stronger pressure wave than dry ablation over the entire radiant exposures [see Fig. 7(a)]. At low radiant exposures, the pressure amplitude of the wet condition was found to be approximately twice that of the dry [see Fig. 7(b)]. It is noted that a transition
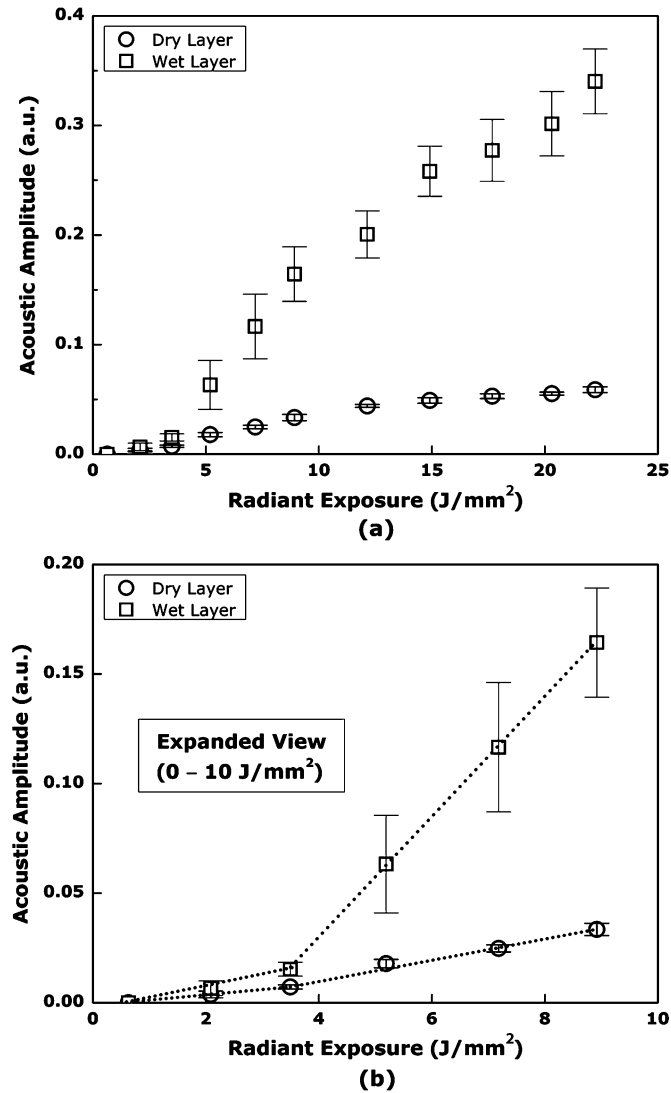
Fig. 7. Comparison of acoustic amplitudes for dry and wet cases as a function of radiant exposure ($n = 10$). (a) Entire radiant exposure and (b) lower radiant exposures between 0 and 10 J/mm^2 expanded from (a) (the dotted lines guide a signal trend of each case).

Fig. 8. Temporal laser pulse and plasma transient detected by a fast photodetector for dry and wet cases at the radiant exposure $H = 17.7$ J/mm^2 on the time scale ranging (a) from 0 to 80 ns and (b) from 0 to 2.25 μs (entire signal trace).

in peak amplitude comparison between the two cases was found at the radiant exposure of 3.5 J/mm^2.

The onset of optical breakdown was observed with a Q-switched Nd:YAG laser by varying the applied pulse energy on bone samples. The breakdown process was evidenced by plasma luminescence and an audible noise from acoustic wave generation. Temporal behavior of the optical pulse and laser-induced plasma for dry and wet cases are shown in Fig. 8. It can be seen in both cases that the plasma developed within approximately 4 ns of the incident laser pulse [see Fig. 8(a)]. The plasma signal exhibited a profile that initially resembled the envelope of the laser pulse, and it reached peak intensity in ∼20 ns regardless of the radiant exposure. Both signals showed the plasma exponential decay after the peak, and, later, the plasma luminescence was suddenly quenched, followed by a secondary exponential component [see Fig. 8(b)]. It is also noted that, after approximately 50 ns, dry and wet cases began to yield different temporal behaviors of plasma evolution. Beyond
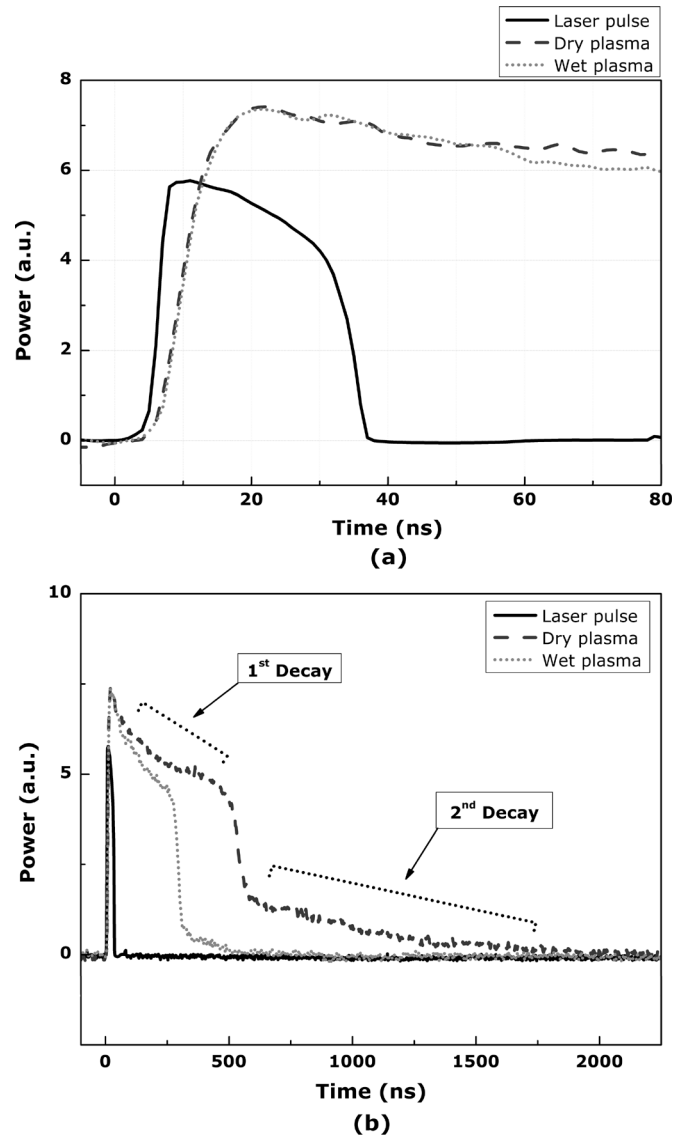
50 ns, plasma generated during wet ablation displayed a faster decay time, converging to the reference state more rapidly, compared with that of dry ablation. Various decay constants for both dry and wet cases were estimated by means of exponential decay curve-fitting ($y = y_0 + A \cdot \exp[-(x - x_0)/\tau]$, y_0: offset, A: amplitude, x_0: center, τ: decay constant), shown in Fig. 9(a). In general, the plasma decay time linearly increased with radiant exposure, and the first plasma decay was up to five times faster than the second decay. Compared with the dry case, the plasma intensity dropped more rapidly during the wet ablation. Fig. 9(b) shows the comparison of plasma duration between two cases as a function of radiant exposure ($n = 10$). The plasma thresholds were measured from the extrapolated curves, and two conditions yielded a comparable threshold of 3.5 J/mm^2, which corresponded to the transition in peak acoustic amplitudes [see Fig. 7]. Upon plasma formation, the lifetimes for dry and wet ablation increased with the radiant
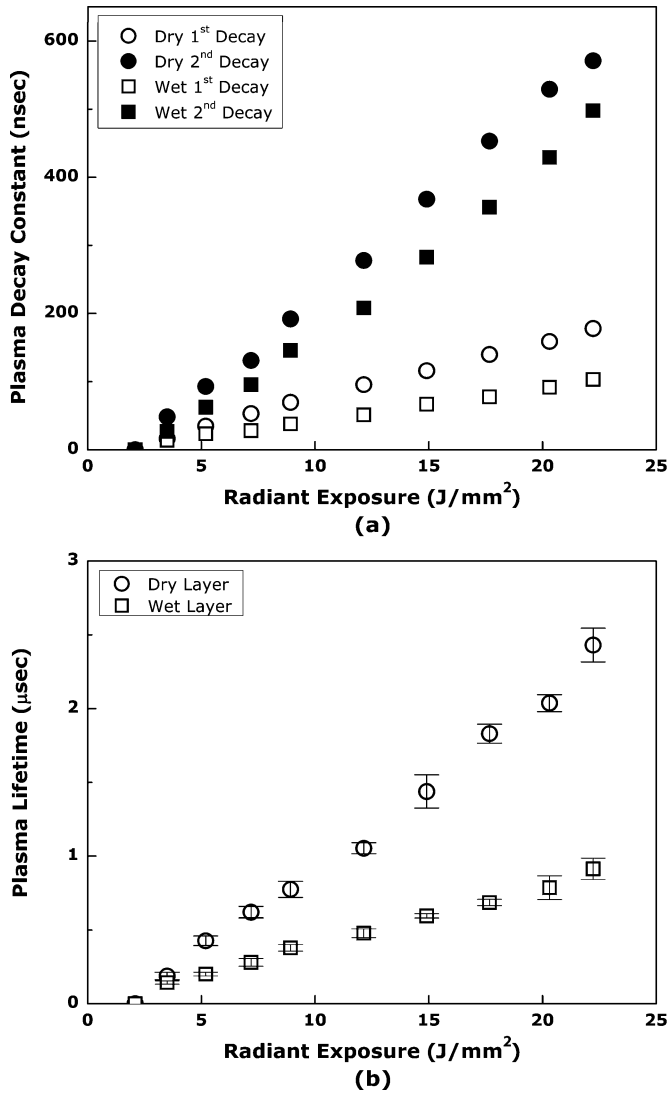
Fig. 9. Comparison of laser-induced plasma between dry and wet cases. (a) Plasma decay constant and (b) plasma lifetime ($n = 10$).

exposure. At a higher radiant exposure, the plasma of the dry case lasted for a few microseconds, which is up to twice as long as that of the wet [see Fig. 9(b)].

IV. Discussion

Nanosecond laser-induced ablation efficiency of the dry and wet conditions was compared for bovine bone samples as a function of radiant exposure with one, ten, and twenty pulses. Laser ablation assisted by a transparent liquid-layer-enhanced ablation efficiency compared to direct irradiation [see Fig. 3]. Craters up to three times deeper with up to six times greater volume were observed under the wet condition. Asymmetric crater shapes with irregular contours, shown in Fig. 2, evidenced photomechanical effects during both dry and wet ablation processes. Observation with an optical microscope showed that the single pulse damage thresholds for both dry and wet cases were 3.5 and 2.1 J/mm^2, respectively. The threshold radiant exposures for measurable acoustic excitation were identical for both cases at 2.1 J/mm^2. However, upon pressure wave generation, the acoustic excitation of the wet condition was higher than that

of the dry case over the entire radiant exposure. The measurable plasma was first detected with a radiant exposure of 3.5 J/mm^2 for both cases. It should be noted that the damage threshold of the wet condition corresponded to that of acoustic excitation, whereas the damage threshold of the dry condition was identical with that of plasma initiation.

Laser-induced ablation under the wet condition has been investigated in a few previous studies [12]–[16], [27]–[29]. It was reported that wet ablation lowered the damage threshold, which is defined as the lowest radiant exposure to cause surface deformation, and promoted ablation performance via explosive liquid vaporization for the radiant exposure near the damage threshold [14]. At a higher radiant exposure regime, the plasma confinement in a water environment significantly enhanced the laser-induced acoustic and shock waves, consequently promoting material removal efficiency [12], [13], [15], [16], [27]–[29].

The lower damage threshold of the wet condition agrees well with previous studies [14], [30]. Considering: 1) higher acoustic excitation near the damage threshold and 2) a damage threshold lower than that of plasma formation, the reduced damage threshold of wet ablation can be attributed to the explosive vaporization. Prior to the plasma formation, nanosecond laser light absorption by the sample leads to rapid surface heating. Thus, thermal conduction from the sample surface to the liquid layer increases the water temperature possibly beyond its equilibrium saturation temperature, causing the liquid water to become superheated. When the superheated liquid becomes unstable, it can approach the spinodal limit, which is a critical temperature of 647 K for water. Near the spinodal limit, the liquid experiences a great density fluctuation, consequently giving rise to homogeneous generation of vapor bubbles as well as validating the expectation of explosive vaporization [14], [30]. In the vaporization of the superheated liquid, the pressure inside the bubble P_{ve} should exceed the vapor pressure at equilibrium, which can be estimated to be

$$P_{ve} = P_{sat}(T_l) \cdot \exp\left[\frac{v_l \cdot (P_l - P_{sat}(T_l))}{RT_l}\right] \quad (2)$$

where T_l, P_{sat}, P_l, v_l, and R are the temperature of the superheated liquid, the saturation pressure at the liquid temperature, the pressure of the superheated liquid, specific volume, and gas constant, respectively [31]. As the temperature approaches 0.83 T_c (T_c: thermodynamic critical temperature of water), the pressure calculated in (2) increases close to the saturation pressure at the liquid temperature with intense density fluctuations [32]. Once a vapor bubble grows to a size greater than a critical radius, it grows spontaneously, accompanying spherical shock wave generation [33]. Therefore, as multiple homo- and/or hetero-geneous micro-bubble nuclei rapidly grow and expand, a strong compressive pressure wave can be emitted, which possibly accounts for a contribution to higher acoustic amplitude at the threshold as well as a lower damage (ablation) threshold for wet ablation prior to plasma formation [see Fig. 4 and 7].

The optical breakdown for both dry and wet cases commenced about 4 ns after the laser pulse was applied over the entire radiant exposure, and both plasmas simultaneously reached the peak intensity in ~20 ns [see Fig. 8(a)]. Once

plasma is initiated due to direct light absorption of a sample, the plasma becomes the main absorber of the remaining pulse energy, resulting in plasma expansion [10]. Previous studies reported that the plasma luminescence is almost a replica of the input pulse [34], [35], so the sudden quenching of both plasma signals can be explained by the reproduction of temporal behavior of the pulse, followed by a secondary exponential decay of the order of up to a microsecond [see Fig. 8(b)]. When the plasma was generated, the plasma under wet condition yielded a fast decay after 50 ns in spite of the identical peak time with dry condition. This implies that more energy transfer to the surrounding media was involved in ablation under water compared to the dry case. This dissipation can be attributed to thermal conduction throughout plasma expansion from high-temperature plasma to the surrounding media, which might have started about 15 ns after the applied pulse ended. Due to the fact that thermal conductivity of water ($k_w = 0.611$ W/m $\cdot$ K at 300 K) is higher than that of air ($k_a = 0.0267$ W/m $\cdot$ K at 300 K), more thermal energy during plasma expansion was possibly transferred to a water layer, reducing plasma lifetime in association with a fast decay transient [see Fig. 9(b)]. Since optical breakdown in water requires an irradiance of more than 10^{11} W/cm^2 and the maximum irradiance tested in the current study was 7.41×10^{10} W/cm^2, we assume that plasma formation occurred at the surface of the bone rather than on the water. In addition to the faster decay of plasma in the presence of a liquid layer, it should be noted that an abrupt increase of acoustic excitation was observed at 3.5 J/mm^2 that corresponded to the plasma threshold radiant exposure. The faster decay of plasma and the abrupt increase of acoustic excitation under the wet condition can be explained by the plasma confinement in the liquid layer. It was reported that the laser-induced plasma could be confined in the liquid layer presenting on the target surface, consequently inducing higher pressure amplitude and longer shock wave duration than the dry condition in spite of the partial absorption of the incoming laser pulse by plasma screening [12], [13], [15], [16], [27], [28].

An analytical model was previously developed to predict laser-induced pressures in the confined geometry [27]. A simple one-dimensional (1-D) model described three different phases of the confined plasma process (i.e., laser heating, adiabatic cooling, and plasma expansion) and evaluated the pressure development inside the plasma. The maximum pressure (P_{max}) generated by the laser-induced plasma in water environment was estimated by the following equation:

$$P_{water}(\text{Pa}) = \sqrt{\frac{2\alpha}{2\alpha + 3}} \cdot \sqrt{E_0} \cdot \sqrt{Z_t} \qquad (3)$$

where α is a constant fraction of the internal energy representing the thermal energy and E_0 is the incident laser irradiance (W/cm^2). Z_t is the characteristic impedance (kg/m^{2}s) between the bone sample and the water layer and is given by

$$\frac{1}{Z_t} = \frac{1}{Z_{bone}} + \frac{1}{Z_{water}} \qquad (4)$$

where Z_{bone} and Z_{water} are the impedances of the bone sample and the water, respectively. By assuming a bone density of 1417 kg/m^3 and a speed of sound of 3000 m/s (based on Table I),
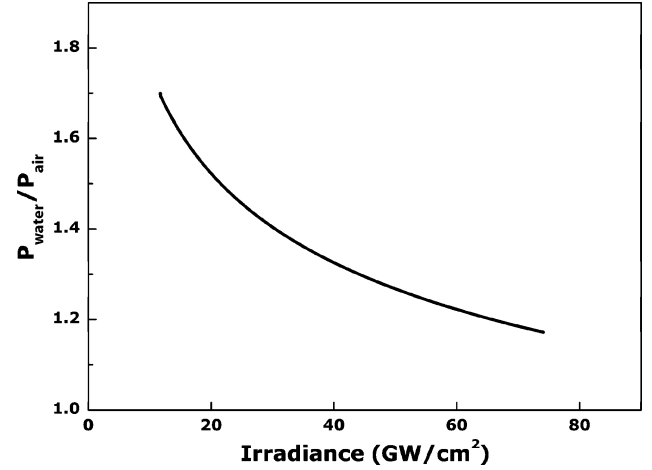

Fig. 10. Ratio of P_{water}/P_{air} based on 1-D analysis of pressure generation induced by plasma process.

$Z_{bone} = 4.251 \times 10^6$ kg/m^{2}s and $Z_{water} = 1.48 \times 10^6$ kg/m^{2}s. For the sake of comparison, the maximum pressure during ablation in air was given by the empirical relation

$$P_{air}(\text{Pa}) = b \cdot E_0^{(n+1)} \cdot \lambda^n \cdot \tau_p^{0.5 \cdot n} \qquad (5)$$

where b and n are material-dependent coefficients, λ is laser wavelength (μm), and τ_p is pulse duration (ns) [27]. Since material removal was photomechanically induced, fracture toughness can be an important parameter to evaluate the susceptibility of bone to initial failure [36]. Material with higher fracture toughness is less likely to fracture by crack propagation; one can assume that the maximum pressure of dry ablation at the plasma threshold is equivalent to the tensile strength applied to crack growth. If $n = -0.3$ based on previous studies and b is determined by the tensile stress estimated from the fracture toughness of bone in Table I, one can approximately obtain that the ratio P_{water}/P_{air} varies from 1.7 to 1.17 over the irradiance range 11.7–74.1 GW/cm^2, shown in Fig. 10. Thus, the liquid confinement appears to achieve higher compressive pressure during plasma formation/expansion over the entire irradiance, which can partially explain a discrepancy in peak acoustic amplitudes between dry and wet ablation in Fig. 7.

Given the fact that the plasma formation for nanosecond pulses is always accompanied with shock wave generation [10], it should be noted that the acoustic impedance of water is $Z_{water} = 1.48 \times 10^6$ kg/m^{2}s, which is much greater than that of air ($Z_{air} = 410$ kg/m^{2}s). If the water–sample interface yields a volumetric space during the plasma expansion, the shock wave is assumed to propagate from the space, which is treated as a perfect gas, to the water layer [27]. Therefore, supposing that air is a perfect gas, the pressure reflection coefficient R for wet ablation is given by

$$R = \frac{Z_{water} - Z_{air}}{Z_{water} + Z_{air}}. \qquad (6)$$

Since R is approximately equal to 1, the induced shock wave propagating out of the sample surface could be mostly reflected

at the interface between air and water without phase change (pressure doubling [20]), so more residual compressive waves were possibly applied to the sample surface [see Fig. 6].

Since the plasma formation is associated with a significant temperature increase, up to 15000 K [37], it is expected that micro-bubble generation emits strong pressure via explosive vaporization in a liquid layer, thus causing additional photomechanical impact. Also, once the bubbles are generated and expanded, they can coalesce into macro-size bubbles. While these macro-bubbles collapse in the vicinity of a surface during/after the ablation process, a high-speed, wall-directed reentrant jet can be initiated in the bubbles, and, consequently, the liquid jet with outward radial flow can interact with the sample as additional shock wave impact [33]. The acoustic augmentation of the jet P_{imp} (Pa) can be estimated using the following equation

$$P_{\mathrm{imp}} = \frac{Z_{\mathrm{bone}} \cdot Z_{\mathrm{water}}}{Z_{\mathrm{bone}} + Z_{\mathrm{water}}} \cdot V_{jet} \qquad (7)$$

where Z_{bone} and Z_{water} are the acoustic impedances of water and bone, respectively ($Z_{\mathrm{bone}} = 4.251 \times 10^6$ kg/m^{2}s and $Z_{\mathrm{water}} = 1.48 \times 10^6$ kg/m^{2}s). If the liquid-jet velocity V_{jet} near a boundary is assumed to be 80 m/s based on a previous study [33], the acoustic impact can correspond to a pressure of 90 MPa, which exceeds the fracture toughness of the bone sample. Therefore, the acoustic enhancement by cavitation bubble collapses can also account for the more pronounced amplitude of the acoustic transient over the entire radiant exposure. It was observed that the liquid vapors were explosively ejected at higher radiant exposure. Hence, in the plasma regime, a combination of confined plasma, impedance difference at the interface, more explosive vaporization, and jet formation can be responsible for the augmentation of compressive pressure along with longer shock wave durations, leading to enhanced photomechanical effects [see Fig. 6]. Future measurement of acoustic signals beyond the 10-μs time frame will clarify how cavitation collapse after plasma expansion contributes to the wet ablation process.

In the case of dry ablation, the acoustic threshold was lower than the damage threshold at 3.5 J/mm^2. Thus, the initial pressure emission resulted from thermoelastic expansion at a radiant exposure of 2.1 J/mm^2, which was below sample damage. Upon plasma initiation at 3.5 J/mm^2 [see Fig. 9], the acoustic emission was assumed to be combined with the thermoelastic wave as well as plasma-induced shock wave generation, subsequently leading to photomechanical damage on the sample. In addition, since the sample was kept in a saline solution at room temperature prior to experimentation, a rapid temperature increase by light absorption possibly induced internal explosion of the interstitial water inside the bone as a mechanical impact. Therefore, it is supposed that material removal for the dry case was mainly attributed to plasma formation, and the acoustic transient was associated with a combination of thermoelastic pressure, plasma-induced shock wave, and recoil momentum. In order to confirm the dynamics implied with the acoustic transient and post-ablation process, high-speed imaging of both dry and wet cases will be performed in the future study.

In Fig. 3, ablation depth and efficiency for both the dry and wet cases started saturating at the radiant exposure of 8.9 J/mm^2. Saturation was also found in the acoustic amplitude graph in Fig. 7. One of the possible explanations for this phenomenon is plasma shielding [38], [39]. Once plasma formation starts at the laser focus, the plasma absorbs and scatters further incident laser light, expanding toward the laser beam during the pulse. Since the plasma partially or fully screens the incident pulse, less energy is delivered to the sample for ablation. Increased shielding effect during plasma formation at higher irradiance was thereby responsible for the saturation of the pressure and ablation efficiency observed for our experiments. Additionally, previous studies have experimentally and analytically shown that both maximum pressure and transmission of plasma approached saturation at the same irradiance threshold, which validated the hypothesis that the plasma shielding was attributed to the pressure saturation, consequently limiting the ablation efficiency [12], [13], [27]. In our experiments, although wet ablation obtained up to six times higher peak pressure and greater ablation efficiency, respectively, than the dry case, it should be noted that, above an irradiance of 2.97×10^{10} W/cm^2, plasma shielding played a significant role in limiting ablation performance. Therefore, an efficient bone ablation rate with a liquid confinement can be achieved below the irradiance of increased plasma shielding effect.

V. CONCLUSION

Biological hard tissue ablation in a liquid confinement has been investigated with a Q-switched Nd:YAG laser. It was found that the application of a water layer increased the ablation efficiency up to six times via explosive liquid vaporization and plasma confinement. The correlation between acoustic and damage thresholds under the wet condition suggests that the explosive vaporization of the superheated liquid was responsible for the lower damage (ablation) threshold along with the higher acoustic amplitude in the near-threshold regime. In the plasma regime, the reduced lifetime of plasma indicates that the optical breakdown was confined to the liquid layer, consequently intensifying acoustic coupling efficiency at the interface. Two other mechanisms have been proposed for the enhanced photomechanical excitation. The augmented photomechanical effect under the wet condition is considered to be the main cause of the improved ablation performance. Above an irradiance of 2.97×10^{10} W/cm^2, acoustic pressure and ablation efficiency were maintained at the saturation level, which was attributed to increased plasma shielding effects. It can be concluded that the liquid layer on the target surface facilitates the augmentation of bone ablation efficiency although it accompanies a limitation of plasma shielding.

REFERENCES

[1] J. H. Moore, *Laser Energy in Orthopedic Surgery*. Amsterdam, The Netherlands: Excerpta Medica, 1973.

[2] L. Clayman, T. Fuller, and H. Becnman, "Healing of continuous-wave and rapid superpulsed carbon dioxide laser-induced bone defects," *J. Oral Maxillofac. Surg.*, vol. 36, pp. 932–937, 1978.

[3] G. K. H. Eyrich, "Laser-osteotomy induced changes in bone," *Med. Laser Appl.*, vol. 20, pp. 25–36, 2005.

[4] G. M. Peavy, L. Reinisch, J. T. Payne, and V. Venugopalan, "Comparison of cortical bone ablations by using infrared laser wavelengths 2.9 to 9.2 μm," *Lasers Surg. Med.*, vol. 26, pp. 421–434, 1999.

[5] M. Forrer, M. Frenz, V. Romano, H. J. Altermatt, H. P. Weber, A. Silenok, M. Istomyn, and V. I. Konov, "Bone-ablation mechanism using CO_2 lasers of different pulse duration and wavelength," *Appl. Phys. B*, vol. 56, pp. 104–112, 1993.

[6] J. A. Izatt, N. D. Sankey, F. Partovi, M. Fitzmaurice, R. P. Rava, I. Itzkan, and M. S. Feld, "Ablation of calcified biological tissue using pulsed laser hydrogen fluoride laser radiation," *IEEE J. Quantum Electron.*, vol. 26, no. 12, pp. 2261–2270, Dec. 1990.

[7] M. S. Kitai, E. N. Sobol, A. P. Sviridov, and A. I. Omel'chenko, "Manifestations of photochemical reactions in bone tissue on exposure to the ultraviolet radiation of an Eximer laser," *Biophysics*, vol. 41, pp. 1151–1157, 1996.

[8] J. T. Walsh, T. J. Flotte, and T. F. Deutsch, "Er:YAG laser ablation of tissue: effect of pulse duration and tissue type on thermal damage," *Lasers Surg. Med.*, vol. 9, pp. 314–326, 1989.

[9] B. Wong, V. Sung, M. W. Berns, L. O. Svaasand, and J. Neev, "Holmium-YAG laser ablation characteristics in calvarial lamellar and cortical bone: the role of water and tissue micro-architecture," *Lasers Med. Sci.*, vol. 10, pp. 181–188, 1995.

[10] M. H. Niemz, *Laser-Tissue Interactions*. Berlin, Germany: Springer-Verlag, 1996.

[11] S. L. Jacques, "Role of tissue optics and pulse duration on tissue effects during high-power laser irradiation," *Appl. Opt.*, vol. 32, pp. 2447–2454, 1992.

[12] L. Berthe, R. Fabbro, P. Peyre, L. Tollier, and E. Bartnicki, "Shock waves from a water-confined laser-generated plasma," *J. Appl. Phys.*, vol. 82, pp. 2826–2832, 1997.

[13] L. Berthe, R. Fabbro, P. Peyre, and E. Bartnicki, "Wavelength dependent of laser shock-wave generation in the water-confinement regime," *J. Appl. Phys.*, vol. 85, no. 11, pp. 7552–7555, 1999.

[14] D. Kim, B. Oh, and H. Lee, "Effect of liquid film on near-threshold laser ablation of a solid surface," *Appl. Surf. Sci.*, vol. 222, pp. 138–147, 2004.

[15] A. Dupont, P. Caminat, and P. Bournot, "Enhancement of material ablation using 248, 308, 532, 1064 nm laser pulse with a water film on the treated surface," *J. Appl. Phys.*, vol. 78, pp. 2022–2028, 1995.

[16] S. Zhu, Y. F. Lu, M. H. Hong, and X. Y. Chen, "Laser ablation of solid substrates in water and ambient air," *J. Appl. Phys.*, vol. 89, pp. 2400–2403, 2001.

[17] G. M. Hale and M. R. Querry, "Optical constants of water in the 200 nm to 200 μm wavelength region," *Appl. Opt.*, vol. 12, pp. 555–563, 1973.

[18] A. Vogel, J. Noack, K. Nahen, D. Theisen, S. Busch, U. Parlitz, D. X. Hammer, G. D. Noojin, B. A. Rockwell, and R. Birngruber, "Energy balance of optical breakdown in water at nanosecond to femtosecond time scales," *Appl. Phys. B*, vol. 68, pp. 271–280, 1999.

[19] F. A. Duck, *Physical Properties of Tissue: A Comprehensive Reference Book*. London, U.K.: Academic, 1991.

[20] D. T. Blackstock, *Fundamentals of Physical Acoustics*. New York: Wiley, 2000.

[21] A. F. Mills, *Basic Heat and Mass Transfer*. London, U.K.: Prentice-Hall, 1999.

[22] J. A. Evans and M. B. Tavakoli, "Ultrasonic attenuation and velocity in bone," *Phys. Med. Biol.*, vol. 35, pp. 1387–1396, 1990.

[23] K. A. Athanasiou, C. F. Zhu, D. R. Lanctot, C. M. Agrawal, and X. Wang, "Fundamentals of biomechanics in tissue engineering of bone," *Tissue Eng.*, vol. 6, pp. 361–381, 2000.

[24] A. E. Siegman, M. W. Sasnett, and T. F. Johnston, Jr., "Choice of clip levels for beam width measurements using knife-edge techniques," *IEEE J. Quantum Electron.*, vol. 27, no. 4, pp. 1098–1104, Apr. 1991.

[25] D. Huang, E. A. Swanson, C. P. Lin, J. S. Schuman, W. G. Stinson, W. Change, M. R. H. , T. J. Flotte, K. Gregory, C. A. Puliafito, and J. G. Fujimoto, "Optical coherence tomography," *Science*, vol. 254, pp. 1178–1181, 1991, JG.

[26] J. A. Izatt, M. D. Kulkarni, S. Yazdanfar, J. K. Barton, and A. J. Welch, "In vivo bidirectional color doppler flow imaging of picoliter blood volumes using optical coherence tomography," *Opt. Lett.*, vol. 22, pp. 1439–1441, 1997.

[27] R. Fabbro, J. Fournier, P. Ballard, D. Devaux, and J. Virmont, "Physical study of laser-produced plasma in confined geometry," *J. Appl. Phys.*, vol. 68, pp. 775–784, 1990.

[28] D. Devaux, R. Fabbro, L. Tollier, and E. Bartnicki, "Generation of shock waves by laser-induced plasma in confined geometry," *J. Appl. Phys.*, vol. 74, pp. 2268–2273, 1993.

[29] S. Zhu, Y. F. Lu, and M. H. Hong, "Laser ablation of solid substrates in a water-confined environment," *Appl. Phys. Lett.*, vol. 79, pp. 1396–1398, 2001.

[30] D. Kim and H. Lee, "Enhanced ablation and photoacoustic excitation in near-threshold laser ablation of liquid-coated surfaces," *J. Appl. Phys.*, vol. 89, pp. 5703–5706, 2001.

[31] V. P. Carey, *Liquid-vapor Phase-Change Phenomena*. Washington, DC: Hemisphere, 1992.

[32] R. Kelly and A. Miotello, "Comments on explosive mechanisms of laser sputtering," *Appl. Surf. Sci.*, vol. 96–98, pp. 205–215, 1996.

[33] J. C. Isselin, A. P. Alloncle, and M. Autric, "On laser induced single bubble near a solid boundary: Contribution to the understanding of erosion phenomena," *J. Appl. Phys.*, vol. 84, pp. 5766–5771, 1998.

[34] F. Docchio, "Lifetimes of plasmas induced in liquids and ocular media by single Nd:YAG laser pulses of different duration," *Europhys. Lett.*, vol. 6, pp. 407–412, 1988.

[35] F. Docchio, P. Regondi, M. R. C. Capon, and J. Mellerio, "Study of the temporal and spatial dynamics of plasmas induced in liquids by nanosecond Nd:YAG laser pulses. 2: Plasma luminescence and shielding," *Appl. Opt.*, vol. 27, pp. 3669–3674, 1988.

[36] P. Zhong, C. Chuong, and G. Preminger, "Characterization of fracture toughness of renal calculi using a microindentation technique," *J. Mater. Sci. Lett.*, vol. 12, pp. 1460–1462, 1993.

[37] P. A. Barnes and K. E. Rieckhoff, "Laser induced underwater sparks," *Appl. Phys. Lett.*, vol. 13, pp. 282–284, 1968.

[38] F. Docchio, P. Regondi, M. R. C. Capon, and J. Mellerio, "Study of the temporal and spatial dynamics of plasmas induced in liquids by nanosecond Nd:YAG laser pulses. 1: Analysis of the plasma starting times," *Appl. Opt.*, vol. 27, pp. 3661–3668, 1988.

[39] A. Vogel, K. Nahen, D. Theisen, and J. Noack, "Plasma formation in water by picosecond and nanosecond Nd:YAG laser pulses—Part I: Optical breakdown at threshold and superthreshold irradiance," *IEEE J. Sel. Topics Quantum Electron.*, vol. 2, no. 4, pp. 847–860, Dec. 1996.
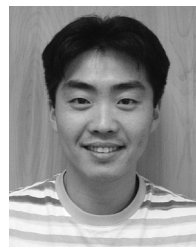
Hyun Wook Kang received the B.S, degree from Yonsei University, Seoul, Korea, in 2002, and the M.S. degree from the University of Texas at Austin in 2005, both in mechanical engineering. He is currently working toward the Ph.D. degree in biomedical engineering at the University of Texas at Austin.

His research interests include mechanisms of pulsed laser ablation of biological tissue, the use of optical coherence tomography, biomedical optics, laser lithotripsy, the endoscopic application of optical fibers, and laser material processing with an emphasis of biomedical applications.

Ho Lee was born in Busan, Korea, on January 4, 1973. He received the B.S. and M.S. degrees from Busan National University, Busan, Korea, in 1996 and 1998, respectively, and the Ph.D. degree from the University of Texas at Austin in 2004, all in mechanical engineering.

He was a Postdoctoral Research Associate with the Wellman Center for Photomedicine, Massachusetts General Hospital, and is currently an Assistant Professor with the School of Mechanical Engineering, Kungpook National University, Daegu, South Korea. His research interests include laser–tissue interactions and therapeutic and diagnostic uses of optics and lasers.

Shaochen Chen received the Ph.D. degree in mechanical engineering from the University of California, Berkeley, in 1999.

Currently, he is an Associate Professor with the Mechanical Engineering Department, University of Texas at Austin. His research interest lies in nanophotonics and laser nanomanufacturing, MEMS/NEMS, and thermal/fluid transport. He teaches a graduate course, ME381R-"MEMS/NEMS," at the University of Texas at Austin.

Dr. Chen received the CAREER award from the National Science Foundation in 2001, the Outstanding Young Manufacturing Engineer award from the Society of Manufacturing Engineers in 2002, and the Young Investigator award from the US Office of Naval Research in 2004. He is a committee member of the ASME Nanotechnology Institute and the IEEE Nanotechnology Council. He is also on the technical committee for NEMS/MEMS packaging of the Electronics and Photonics Packaging division (EPPD) of ASME. He served as a Guest Editor in 2003 for the IEEE TRANSACTIONS ON ADVANCED PACKAGING Special Issue on NEMS/MEMS Packaging.

Ashley J. Welch received the B.E. degree from Texas Tech University, Lubbock, in 1955, the M.S. degree from Southern Methodist University, Dallas, TX, in 1959, and the Ph.D. degree from Rice University, Houston, TX, in 1964, all in electrical engineering.

He is currently a Professor of Biomedical Engineering and is the Marion E. Forsman Centennial Professor in Engineering with the University of Texas at Austin. He joined the University of Texas at Austin as an Assistant Professor in 1964. He is an international authority on the optical and thermal response of tissue to laser irradiation. His current research include fundamental analysis of laser-tissue interaction, OCT imaging, the application of hyperosmotic agents in reducing light scattering, laser lithotripsy, and the investigation of short pulse tissue ablation. He has published over 350 papers and book chapters describing his research.